HHS Public Access

Author manuscript

J Neurosci Methods. Author manuscript; available in PMC 2020 January 01.

Published in final edited form as:

J Neurosci Methods. 2019 January 01; 311: 76–82. doi:10.1016/j.jneumeth.2018.10.005.

Electrokinetic Infusions into Hydrogels and Brain Tissue: Control of Direction and Magnitude of Solute Delivery.

Amir H. Faraji[1,2], **Andrea S. Jaquins-Gerstl**[1], **Alec C. Valenta**[1], and **Stephen G. Weber**[1]

[1]Department of Chemistry, 219 Parkman Avenue, Chevron Science Center, University of Pittsburgh, Pittsburgh, Pennsylvania 15213 USA;

[2]Department of Neurological Surgery, 200 Lothrop Street, UPMC Presbyterian Hospital, Pittsburgh, Pennsylvania 15213 USA

Abstract

Background: Delivering solutes to a particular region of the brain is currently achieved by iontophoresis for very small volumes and by diffusion from a microdialysis probe for larger volumes. There is a need to deliver solutes to particular areas with more control than is possible with existing methods.

New Method: Electrokinetic infusions of solutes were performed into hydrogels and organotypic hippocampal slice cultures. Application of an electrical current creates electroosmotic flow and electrophoresis of a dicationic fluorescent solute through organotypic hippocampal tissue cultures or larger hydrogels. Transport was recorded with fluorescence microscopy imaging in real-time.

Results: Electrokinetic transport in brain tissue slice cultures and hydrogels occurs along an electrical current path and allows for anisotropic delivery over distances from several hundred micrometers to millimeters. Directional transport may be controlled by altering the current path. The applied electrical current linearly affects the measured solute fluorescence in our model system following infusions.

Comparison with Existing Methods: Localized drug delivery involves iontophoresis, with diffusion primarily occurring beyond infusion capillaries under current protocols. Pressure-driven infusions for intraparenchymal targets have also been conducted. Superfusion across a tissue surface provides modest penetration, however is unable to impact deeper targets. In general, control over intraparenchymal drug delivery has been difficult to achieve. Electrokinetic transport provides an alternative to deliver solutes along an electrical current path in tissue.

Corresponding Author Stephen G. Weber, 219 Parkman Avenue, Chevron Science Center, University of Pittsburgh, Pittsburgh, Pennsylvania 15213 USA; Phone (412) 624-8520.

CONFLICT OF INTEREST

Declarations of interest: none.

Conclusions: Electrokinetic transport may be applied to living systems for molecular transport. It may be used to improve upon the control of solute delivery over that of pressure-driven transport.

Graphical Abstract

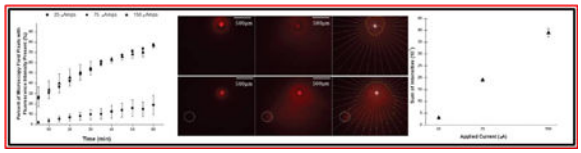

Keywords

Electrokinetic Transport; Drug Delivery; Iontophoresis; Electroosmosis

1. INTRODUCTION

Iontophoresis performed from a capillary tip into the brain uses short electrical current pulses (milliseconds to seconds) and occurs over very short distances (nanometers to a few micrometers) to impact a single or few neurons or cells for study. [1, 2] Thus, iontophoresis can deliver a molecule into the brain, but within the tissue it is primarily diffusion that determines the ultimate distribution of the solute delivered. [3-6] We previously reported that electrokinetic transport includes components of both electroosmosis and electrophoresis.[7] Electroosmosis is initiated through the effect of an electric field on mobile counterions that are loosely associated with a charged, porous framework containing the interstitial fluid. Water molecules interact transiently with the moving counterions and momentum is transferred to the fluid itself resulting in bulk fluid flow. In brain tissue, the cells' exterior surfaces and extracellular matrix represents a "charged, porous framework." The only measurement relating to this was demonstrated in organotypic hippocampal slice cultures (OHSCs) and established that electroosmotic flow is significant and in the same direction as the electrophoresis of cations. [8, 9] Electrophoresis is the movement of ions resulting from the force of the electrical potential gradient on the charge of the ion.

We have demonstrated the role of electrokinetic transport in long-time iontophoresis, in which molecules were infused and conveyed over distances up to a several hundred micrometers from micrometer-sized iontophoresis pipettes using sustained current application times,[7] which were longer than times traditionally used in neurochemical applications of iontophoresis.[1] A semi-empirical equation was further devised to model the quasi-steady-state infusion profile of a solute outside of a cannula tip due to electrokinetic transport in a porous medium, including the contributions from electrophoresis, electroosmosis, and diffusion.[7, 10]

In addition, we have extensively studied the role of electrokinetic transport on perfusing brain tissue and capturing the perfusate for *in vitro* analysis. These experiments used electrical currents to perfuse the extracellular space with a peptide and collect the perfusate containing products of peptide hydrolysis for determination of aminopeptidase activity.[11, 12] This work demonstrated that electrokinetic transport of a molecule into and through

porous, aqueous media - hydrogels and OHSCs - depends on individual properties of the infused solute (such as its electrophoretic mobility and size), the conductivity of the carrier fluid used during the infusion, the applied electrical current, and specific properties of the tissue or gel (such as the medium's tortuosity and ζ-potential). [9] However, the volumes affected by the delivery were still quite small.[10]

Iontophoresis has also been used to move molecules through a barrier such as the skin or sclera into the underlying tissue. [13, 14] Localized drug delivery to OHSCs has also been performed by superfusion using a multifunctional pipette based on pressure-flow from a microfluidic system to control flow rates through the pipette.[15] This system was used to superfuse OHSCs along a single dendritic layer with detection up to several hundred micrometers away for neurochemical analysis. This methodology, however, is limited by its reliance upon diffusion from the surface into the OHSCs.

Finally, while sustained pressure-driven infusions of solutes into the brain is not commonly used in research, it was first described to introduce macromolecules and small molecules into the brains of cats with locally high concentrations.[16] The initial infusions predominately occurred within the white matter (less dense, higher porosity) with subsequent partition into the gray matter (more dense, lower porosity) in a delayed fashion. As this methodology was explored over more than two decades to the present date, the rates of infusion, infusion cannula size, infusate concentrations, and pre-infusion sealing times to allow for accommodation of the infusion cannula were systematically studied.[17-22]

Despite these advances, increased control of an infusate is highly desired in both the laboratory and eventually in clinical practice. This work examines the effect of an electrical current on the path of electrokinetic transport in OHSCs and hydrogel models of brain tissue. We examine the impact of altering the electrical current on the extent of infusion, and further comment on avenues for future investigation, including the influence of an applied electrical current on neuronal tissue. Electrokinetic transport may be able to provide a greater ability to direct molecules along electrical current paths in neuronal tissue for applications to both laboratory and clinical practice.

2. MATERIALS AND METHODS

2.1 Chemicals and Solutions

The following materials were purchased from Sigma (St. Louis, MO) and used as received, unless otherwise noted. Solutions were prepared with Millipore Synthesis A10 system 18 MΩ purified water (Millipore, Billerica, MA). Glucose-free HEPES-buffered salt solution (GF-HBSS) contained in mM: 143.4 NaCl, 5 HEPES, 5.4 KCl, 1.2 $MgSO_4$, 1.2 NaH_2PO_4, and 2.0 $CaCl_2$. GF-HBSS was filtered, stored frozen, warmed to room temperature, and ultrasonicated for ten minutes prior to use. HBSS contained the same component concentrations as GF-HBSS, with an additional 10 mM *D*- (+)-glucose, and underwent the same preparation and storage process. GBSS was made up of 27.5 mM *D*-(+)-glucose and 2.7 mM $MgSO_4$ supplemented to Gey's Balanced Salt solution. GBSS was filtered, stored in the refrigerator, and warmed to 37 °C prior to use. The OHSC culture medium contained the following components from Gibco (Invitrogen, Eugene, OR): 50% Opti-MEM, 25% heat-

inactivated Horse Serum, and 25% Hanks' Balanced Salt Solution, supplemented with 2% vitamin B-27 and 1% *D*-(+)-glucose.[23] The medium was filtered, stored in the refrigerator, and warmed to 37 °C prior to use. The chloride salt of tris(2,2'-bipyridine)ruthenium (abbreviated $Ru(bpy)_3^{2+}$) was obtained from Sigma and diluted to make a solutions of 1.3 mM $Ru(bpy)_3^{2+}$ in 150 mM aqueous NaCl supplemented with 5 mM HEPES buffered at pH 7.4.

2.2 Organotypic Hippocampal Slice Cultures (OHSCs)

This procedure was approved by the University of Pittsburgh Institutional Animal Care and Use Committee and follows the directives in the National Institutes of Health guide for the care and use of Laboratory animals (NIH Publications No. 8023, revised 1978). The organotypic hippocampal slice culture (OHSC) method was developed by Stoppini *et al.,* [24] and used with slight modification. Bilateral dissections of the hippocampi were done on 9-day postnatal Sprague-Dawley albino rat pups. The hippocampi were chopped along their transverse axes using a McIlwain tissue chopper (Mickle Laboratory Engineering, Surrey, England) to yield 350μm thick slices. The slices were positioned on 0.4μm PTFE insert membranes (Millipore, Bedford, MA) and incubated over 1.2 mL of culture medium at 36.5 °C in 5 % CO_2/95 % air for 6 to 8 days. The culture medium was exchanged every 2 to 3 days. Prior to use, the culture medium was replaced by 37 °C GBSS and incubated for thirty minutes. A second exchange of GBSS and incubation for another 30 minutes was followed by a final exchange to 37 °C HBSS and incubated for 30 minutes prior to experiments. OHSCs were approximately 160μm in thickness following incubation.[25]

2.3 Electrokinetic Infusions into Hydrogels

Hydrogel pieces were synthesized,[26] cut, and placed in the experimental cell. The hydrogel thickness was greater than 5 mm in all instances. Fused silica capillaries were used as the infusion and counter capillaries. Fused silica capillaries of 101.6 ± 0.4μm inner diameter, 361.1 ± 0.9 μm outer diameter, and 10 cm length were cleanly cut to blunt tips. One capillary (dye capillary) was filled with $Ru(bpy)_3^{2+}$ while another capillary (counter capillary) was filled with GF-HBSS. A Digital Midgard™ Precision Current Source iontophoretic pump (Stoelting Co., Wood Dale, IL) or Princeton Applied Research 173 potentiostat (PAR) (Princeton, NJ) were used as the constant current source. The current source was attached to the secured Ag electrodes through a circuit containing a relay switch, as reported previously.[7] The cell was affixed to an Olympus IX-71 or IX-81 inverted fluorescence microscope stage, and experiments were imaged with a high-resolution charged-coupled device camera (ORCA-ER). Image sequences were acquired using MetaMorph 7.6.2.0 software (MDS Analytical Technologies, Sunnyvale, Ca) using an UPlan Fl 1.25×, NA 0.04 Olympus objective lens. For $Ru(bpy)_3^{2+}$ images, the excitation wavelength was 452 nm and the emission wavelength was 620 nm. The MetaMorph software triggered the initiation and termination of the current during image acquisition. The Midgard™ pump or the PAR potentiostat monitored the electrical potential across the system as a constant current was applied.

2.4 Electrokinetic Infusions into OHSCs

Experiments in the OHSCs were conducted with the Digital Midgard™ iontophoresis pump as the constant current source. An insert membrane with an OHSC was placed in a glass dish with HBSS. A silver wire ground electrode was secured remotely and immersed in the HBSS bath or placed in the OHSC. A fused silica capillary was filled with a fluorophore solution and positioned perpendicular to the plane of the OHSC and insert membrane using a manipulator arm affixed to a Narishige NMN-21 micromanipulator (Tokyo, Japan). The capillary were also 101.6 ± 0.4 μm inner diameter and 361.1 ± 0.9 μm outer diameter. The capillary tip was introduced into the CA1 region of the OHSC. The electrode circuitry and imaging parameters were otherwise analogous to the hydrogel experiments.[7]

The penetration distance was obtained from image sequences by utilizing line scans from the center of the capillary tip to the edge of the viewfield on the same plane as the injection capillary. The intensity data were recorded along the line scan prior to the initiation of current (to obtain the background intensity) and at 30 seconds intervals following initiation of the current. The background intensity was subtracted from the corresponding intensity along the line scan and 25% and 15% of the maximal intensity were documented to create an “iso-concentration” contour. The reported fluorescence intensity values are between 0 and 4,095.

2.5 Surface Intensity Plots

For quantitative image analysis, NIS Elements Advanced Research software version 4.0 (Nikon Instruments, Inc.), was used to convert the $Ru(bpy)_3^{2+}$ images to color-coded surface intensity plots. All images were first thresholded using a built-in function in NIS Elements software; this removes the background but does not affect other features of the image.[27] The intensity range was 0-255 (low-high). A color bar was used to represent relative intensity with white (255) and black (0). Color coded surface intensity plots were used to analysis dye movement and intensity.

2.6 Percent of Microscopy Field Pixels with Fluorescence Intensity Present Plot

The percentage of pixels with $Ru(bpy)_3^{2+}$ present was determined for each approximately 160 μm tissue slice or hydrogel using NIS Elements Advanced Research software version 4.0 (Nikon Instruments, Inc.). Each image was thresholded against background levels and the region of interest (ROI) was selected. This area’s pixel count was expressed as a percent of the total pixel count using the binary-threshold tool of NIS Elements. Experiments with each current were performed three times. Similarly, the aggregate or total fluorescence intensity within the viewing area was background-subtracted and used as a surrogate to compare gross movement of fluorophore into the matrix from infusion capillary.

2.7 Sum of Fluorescence Intensity Plot

The sum of intensities over the pixels within the ROI was determined similarly to the above. Using the binary-threshold tool of NIS Elements the sum of individual pixel counts within the ROI was calculated for each image. Experiments were carried out in triplicate at each current.

3. RESULTS AND DISCUSSION

3.1 Electrokinetic Transport is Determined by Current Path in Hydrogel Models

A family of poly(acrylamide-co-acrylic acid) hydrogels was developed and previously validated to provide a robust model system to test the effect of electrokinetic transport during delivery into a matrix of interest. [26] These hydrogels have a ζ-potential similar to the OHSCs (about −25 mV). We sought to control solute transport by setting up clearly defined current paths using capillaries with approximately 100 μm diameter openings and using $Ru(bpy)_3^{2+}$, a small, dicationic fluorescent solute with a known electrophoretic mobility. [8, 9] Fig. 1A shows the infusion capillary (right) and counter capillary/electrode (left) in a hydrogel spaced 4 mm apart. A 75 μA current was applied across the hydrogel for one hour. The ability to direct the path of the fluorescent dye $Ru(bpy)_3^{2+}$ towards the counter capillary is demonstrated in Fig. 1.

Prior to applying the electrical current, fluorescence from $Ru(bpy)_3^{2+}$ is only observed to come from the source capillary lumen. When the current was applied, the dye moved through the hydrogel towards the counter capillary along its current path in an anisotropic manner, as shown by the surface intensity plots. This was not observed in the control experiment with no current applied. This provides evidence that electrokinetic transport may occur in an anisotropic manner along a current path.

3.2 Electrokinetic Transport is Determined by Current Path in OHSCs

To demonstrate how the current path may impact the directionality of electrokinetic transport in OHSCs, experiments were performed with 100 μm inner diameter fused silica capillaries containing $Ru(bpy)_3^{2+}$ placed perpendicularly into CA1 of an OHSC with the counter electrode in two different areas in separate experiments. The counter electrode (0.3 mm diameter Ag wire) was placed in either the buffer solution below the tissue or inserted into CA3 of an OHSC with no buffer below it. In the control experiment (counter electrode in the buffer), the fluorescence was situated around the cannula tip in an isotropic manner, with decreased fluorescence within the OHSC after a 1.5 μA current was applied for 25 minutes (Fig. 2, top row). The bottom row shows the infusion of $Ru(bpy)_3^{2+}$ when the counter electrode is in the tissue with no GF-HBSS below the OHSC insert membrane after 25 minutes of an applied 1.5 μA current. The current path must be through the tissue and the insert membrane and passes from the source to the counter electrode. As such, $Ru(bpy)_3^{2+}$ transport is anisotropically towards the counter electrode, as shown in Fig. 2.

While these observations are certainly not unanticipated, this simple demonstration would be very difficult, if not impossible, with pressure-controlled flow. In addition, the electrical current used in this experiment was much lower than that used in the hydrogel work and on the order of those used with microiontophoresis. Accordingly, the current density is also lower than with electroosmotic sampling yet millimeter-distance transport clearly occurs through the OHSCs. As compared to superfusions with multifunctional pipettes across the surface of OHSCs for localized neurochemical analysis, this methodology transports interstitial fluids at low electrical currents that are readily achievable using standard equipment. Moreover, this method of delivery puts the solute in a region of tissue away from

the delivery source so that the source does not interfere with real-time imaging over the area being analyzed.

3.3 Electrical Current Considerations and Limitations

Both directionality and volume perfused depend on the current magnitude, thus we sought to further increase the flow rate and achieve larger distribution volumes by varying applied currents in poly(acrylamide-*co*-acrylic acid) hydrogels with a homogeneous ζ-potential similar to rat brains as a surrogate. [26] Similar to our previously-described setup for Fig. 1, we applied three currents (25, 75, and 150 μA) across the hydrogels using approximately 100 μm inner diameter fused silica capillaries filled with $Ru(bpy)_3^{2+}$. Images of the evolving infusion zones were acquired every five minutes (1.25×, numerical aperture 0.04) Intensities in each pixel above background were determined (MetaMorph). The number of pixels above background was taken as a measure of the projected area of the infusion volume. The total intensity in those pixels was taken as a further measure of the infused volume. Fig. 3A demonstrates that both the growth of the infused zones over time and the zone shapes are similar for the two larger currents. The intensity measurements (Fig. 3B) demonstrate that there was a significant effect of current on the amount of material infused, as expected.

Higher electrical currents should result in increased infusion volumes, which seems to be corroborated by Fig 3. The electric field decays approximately as $1/r^2$ for infusions from a single point source, which may limit the extent of electrokinetic transport and penetration through the hydrogel or tissue at further distances in the current setup.

Along related lines, bright field microscopy images taken during the electrokinetic infusions demonstrated no visible distortion of the hydrogels or OHSCs due to the electroosmotic infusions. In a homogeneous porous medium, there is no appreciable pressure drop accompanying electroosmotic flow of interstitial fluid or infusate. On the other hand, a pressure gradient should develop at the interface of the two adjacent media with different ζ-potentials. As the capillary and tissue ζ-potentials are different, we expect that a small pressure gradient exists in these perfusions. However, we have not attempted to measure this and have not observed any pressure deformation with microscopy. Thus, molecular delivery may be achieved with electrokinetic transport by passing an electrical current through a source solution into tissue.

Additional considerations involve the safety and compatibility of an applied electrical current in neuronal tissue. In our previous work, no differences in cell death were observed at the infusion site when assessed by propidium iodide staining in OHSCs versus controls. [7] However, it remains unclear whether neuronal function is altered and what electrical current thresholds are truly “safe.” These prior studies utilized higher current densities than those proposed in our current work, and the most profound effects would be experienced near the capillary tip. As an example, the current densities at a 100 μm diameter capillary tip carrying between 1.5 to 25 μA ranges from 191 to 3,180 A/m^2. In contrast, the current density for previously-published 0.5 μA ejections from an 4 μm diameter capillary tip was 39,790 A/m^2 with no visible cell death surrounding the tip. [7] Electroporation from a 2 μm diameter capillary tip with a typical current of 0.125 μA coincidentally also used a current density of 39,790 A/m^2. [28] To achieve similarly high, yet “safe,” electrical current

densities from a 100 μm diameter capillary tip, the applied current would need to be roughly 0.3 mA. In assessing damage from electroosmotic flow through OHSC, the CA1 was more susceptible than CA3, which was much more susceptible than the infrapyramidal blade of the dentate gyrus. [29] Thus, it is likely to be difficult to generalize regarding the effect of a particular current density or electric field on the health of neurons.

Deep brain stimulation (DBS) is a clinical technique to apply an electrical field and stimulate target neurons in a variety of neurological conditions, including Parkinson's disease, tremors, dystonia, and recently, psychiatric disorders.[30-33] A roughly 25.5 mA current passed through a 0.06 cm^2 electrode, as typical of DBS in patients, results in an estimated electrical current density of 4,250 A/m^2.[34] In contrast, the timescale of our experimental electrokinetic infusions is relatively short (approximately an hour or less) versus that of DBS (typically years). It has been postulated that the electrical current, pulse frequency, and duration of treatment are essential to the efficacy of DBS. [30, 31] This is primarily due to modulation of neuronal and non-neuronal activity, which occurs after chronic DBS therapy. Ultimately, the long-term effects of an applied electrical current upon brain tissue remains an area of active clinical and scientific investigation.

Numerous theories exist to explain how application of an electric field (and its frequency, duration, and synchronicity) in neuronal tissue may contribute to alterations in neuronal function or the distribution of endogenous compounds.[35] The duration of time that a neuronal membrane is polarized and the ultimate sensitivity of that membrane to polarization likely determines the actual physiological effect of an applied electrical field. [31] Changes in cellular membrane polarization in the brain can result in alterations in blood-brain barrier integrity, action potential firing and propagation, network coherence, plasticity, and molecular or morphological changes.[35, 36] Moreover, localized electrochemical changes may also occur with sustained electrical current application that perturb the intracellular and extracellular concentrations of endogenous chemicals and their gradients. [31] Of particular concern is the possibility of seizure activation in the brain. Application of direct electrical currents greater than 60 mA across rat brain slices have been shown to trigger action potentials in quiescent cortical cells and epileptiform discharges have been documented in hippocampal slices at electrical currents greater than 500 mA.[37, 38] While these electrical currents are significantly higher than those used in our present study, the current densities utilized in our work is actually higher at regions concentrated around the infusion capillaries. Ultimately these important issues remain an active area of ongoing research.

Finally, it is important to address the contributions of diffusion to transport. As described in Equation 1, the Peclet number, *Pe,* describes the impact of diffusion and is characterized by the effective diffusion coefficient in the tissue, D_{eff}, in the presence of a convective velocity, *v*. [7]

$$\mathrm{Pe} = va/D_{eff} \quad 1$$

The characteristic distance *a,* is chosen to suit the question. We determined in earlier work[7] using electroosmotic infusion capillaries with μm-scale tip openings that the concentration profile of an infused fluorescent dextran into OHSCs was consistent with theory based an electric-field-dependent velocity and thus Pe. We have demonstrated here that convective movement along the electrical current path is significant. The velocity is proportional to the current density, which in our experiments is highest near the infusion capillary and counterelectrode, but is lower at distances between the infusion capillary and the counterelectrode. Therefore, the rate of convective transport is highest near the infusion capillary and counter electrode with a resultantly high Peclet number. The Peclet number decreases as the electric field decays at distances away from the capillary tip and the diffusional contributions to transport become more apparent. However, the observed solute spreading may not necessarily be solely due to molecular diffusion. Solute transport through a porous medium results in dispersion caused by the random orientation of the positions of obstructions (cells, axons, etc.) that defines the direction of the local fluid flow. Contributions from molecular diffusion, but not the dispersion caused by the latter effect, can be reduced by increasing solute velocity either by increasing the electric field or the solute mobility, e.g. by adding positive charge. However, there are practical limitations on both.

4. CONCLUSIONS

The transport of solutes into porous, aqueous media strongly depends on properties of the solute (such as the electrophoretic mobility and molecular weight), the applied electrical current, the flow rate through the infusion capillary tip, and properties outside of the capillary tip, such as the medium's ζ-potential, porosity, and tortuosity. We demonstrate application of a wide array of sustained electrical currents to effect electrokinetic transport in OHSCs and hydrogel models of brain tissue for localized or more widespread infusions. We have further shown that electrokinetic transport occurs along an electrical current path, even for very low currents, and may allow for anisotropic delivery at greater distances than iontophoresis or electroosmotic sampling. There is additional room to increase the applied electrical current and infusion times with this system. Directional control requires an appreciable electrical current; however, the limits of the electrical current will ultimately be dictated by its safety and compatibility in living neuronal tissue. This methodology may be used to enhance the control of pressure-driven delivery and iontophoresis in laboratory research and potentially in clinical practice.

ACKNOWLEDGMENTS

This work was made possible by grant numbers UL1 RR024153 and R01 GM044842 from the National Institutes of Health (NIH). Special thanks to Chuck Fleishaker and Tom Gasmire in the Department of Chemistry electronics and machine shops for their assistance in developing the setup required for these experiments.

REFERENCES

1. Stone TW, ed. Microiontophoresis and Pressure Ejection. Vol. 8 1985, Wiley: Chichester, U.K.
2. LeBeau FE, Malmierca MS, and Rees A, Iontophoresis in vivo demonstrates a key role for GABA(A) and glycinergic inhibition in shaping frequency response areas in the inferior colliculus of guinea pig. J Neurosci, 2001 21(18): p. 7303–12. [PubMed: 11549740]

3. Nicholson C, Phillips JM, and Gardner-Medwin AR, Diffusion from an iontophoretic point source in the brain: role of tortuosity and volume fraction. Brain Res, 1979 169(3): p. 580–4. [PubMed: 445169]
4. Norman RS, Diffusional spread of iontophoretically injected ions. J Theor Biol, 1975 52(1): p. 159–62. [PubMed: 1152479]
5. Kirkpatrick DC and Wightman RM, Evaluation of Drug Concentrations Delivered by Microiontophoresis. Anal Chem, 2016 88(12): p. 6492–9. [PubMed: 27212615]
6. Kirkpatrick DC, et al., Characterization of solute distribution following iontophoresis from a micropipet. Anal Chem, 2014 86(19): p. 9909–16. [PubMed: 25157675]
7. Guy Y, et al., Iontophoresis from a micropipet into a porous medium depends on the zeta-potential of the medium. Anal Chem, 2012 84(5): p. 2179–87. [PubMed: 22264102]
8. Guy Y, et al., Determination of zeta-potential and tortuosity in rat organotypic hippocampal cultures from electroosmotic velocity measurements under feedback control. Anal Chem, 2009 81(8): p. 3001–7. [PubMed: 19298057]
9. Guy Y, Sandberg M, and Weber SG, Determination of zeta-potential in rat organotypic hippocampal cultures. Biophys J, 2008 94(11): p. 4561–9. [PubMed: 18263658]
10. Varner EL, et al., Enhancing Continuous Online Microdialysis Using Dexamethasone: Measurement of Dynamic Neurometabolic Changes during Spreading Depolarization. ACS Chem. Neurosci, 2017 8(8): p. 1779–1788. [PubMed: 28482157]
11. Ou Y and Weber SG, Higher Aminopeptidase Activity Determined by Electroosmotic Push-Pull Perfusion Contributes to Selective Vulnerability of the Hippocampal CA1 Region to Oxygen Glucose Deprivation. ACS Chem Neurosci, 2018 9(3): p. 535–544. [PubMed: 29078045]
12. Ou Y, et al., Electroosmotic perfusion of tissue: sampling the extracellular space and quantitative assessment of membrane-bound enzyme activity in organotypic hippocampal slice cultures. Anal Bioanal Chem, 2014 406(26): p. 6455–68. [PubMed: 25168111]
13. Pikal MJ, The role of electroosmotic flow in transdermal iontophoresis. Adv Drug Deliv Rev, 2001 46(1–3): p. 281–305. [PubMed: 11259844]
14. Hao J, et al., Electrically assisted delivery of macromolecules into the corneal epithelium. Exp Eye Res, 2009 89(6): p. 934–41. [PubMed: 19682448]
15. Ahemaiti A, et al., Spatial characterization of a multifunctional pipette for drug delivery in hippocampal brain slices. J Neurosci Methods, 2015 241: p. 132–6. [PubMed: 25554414]
16. Bobo RH, et al., Convection-enhanced delivery of macromolecules in the brain. Proc Natl Acad Sci U S A, 1994 91(6): p. 2076–80. [PubMed: 8134351]
17. Chen MY, et al., Variables affecting convection-enhanced delivery to the striatum: a systematic examination of rate of infusion, cannula size, infusate concentration, and tissue-cannula sealing time. J Neurosurg, 1999 90(2): p. 315–20. [PubMed: 9950503]
18. Krauze MT, et al., Effects of the perivascular space on convection-enhanced delivery of liposomes in primate putamen. Exp Neurol, 2005 196(1): p. 104–11. [PubMed: 16109410]
19. Baraban SC and Bausch SB, Organotypic Hippocampal Slice Cultures as a Model ofLimbic Epileptogenesis, in Animal Models of Epilepsy. 2009, Humana Press p. 183–201.
20. Richardson RM, et al., Interventional MRI-guidedputaminal delivery of AAV2-GDNF for a planned clinical trial in Parkinson's disease. Mol. Ther, 2011 19(Copyright (C) 2012 American Chemical Society (ACS). All Rights Reserved.): p. 1048–1057. [PubMed: 21343917]
21. Fiandaca MS, et al., Image-guided convection-enhanced delivery platform in the treatment of neurological diseases. Neurotherapeutics, 2008 5(1): p. 123–7. [PubMed: 18164491]
22. Olson JJ, et al., Assessment of a balloon-tipped catheter modified for intracerebral convection-enhanced delivery. J Neurooncol, 2008 89(2): p. 159–68. [PubMed: 18458816]
23. Noraberg J, Kristensen BW, and Zimmer J, Markers for neuronal degeneration in organotypic slice cultures. Brain Res Brain Res Protoc, 1999 3(3): p. 278–90. [PubMed: 9974143]
24. Stoppini L, Buchs PA, and Muller D, A simple method for organotypic cultures of nervous tissue. J Neurosci Methods, 1991 37(2): p. 173–82. [PubMed: 1715499]
25. Guy Y, et al., A simple method for measuring organotypic tissue slice culture thickness. J Neurosci Methods, 2011 199(1): p. 78–81. [PubMed: 21497166]

26. Faraji AH, et al., Synthesis and characterization of a hydrogel with controllable electroosmosis: a potential brain tissue surrogate for electrokinetic transport. Langmuir, 2011 27(22): p. 13635–42. [PubMed: 21905710]
27. Nesbitt KM, et al., Pharmacological mitigation of tissue damage during brain microdialysis. Anal Chem, 2013 85(17): p. 8173–9. [PubMed: 23927692]
28. Agarwal A, et al., Effect of cell size and shape on single-cell electroporation. Anal Chem, 2007 79(10): p. 3589–96. [PubMed: 17444611]
29. Hamsher AE, et al., Minimizing tissue damage in electroosmotic sampling. Anal Chem, 2010 82(15): p. 6370–6. [PubMed: 20698578]
30. Montgomery EB and He H, Deep Brain Stimulation Frequency-A Divining Rod for New and Novel Concepts of Nervous System Function and Therapy. Brain Sci, 2016 6(3).
31. McIntyre CC and Anderson RW, Deep brain stimulation mechanisms: the control of network activity via neurochemistry modulation. J Neurochem, 2016 139 Suppl 1: p. 338–345. [PubMed: 27273305]
32. Wichmann T and Delong MR, Deep brain stimulation for neurologic and neuropsychiatric disorders. Neuron, 2006 52(1): p. 197–204. [PubMed: 17015236]
33. Sharma M, Naik V, and Deogaonkar M, Emerging applications of deep brain stimulation. J Neurosurg Sci, 2016 60(2): p. 242–55. [PubMed: 26788743]
34. Medtronic, Medtronic Kinetra® 7428 Technical Manual - Dual Program Neurostimulator for Deep Brain Stimulation. 2008, Minneapolis, MN.
35. Jackson MP, et al., Animal models of transcranial direct current stimulation: Methods and mechanisms. Clin Neurophysiol, 2016 127(11): p. 3425–3454. [PubMed: 27693941]
36. Yao L, et al., Electric field-guided neuron migration: a novel approach in neurogenesis. Tissue Eng Part B Rev, 2011 17(3): p. 143–53. [PubMed: 21275787]
37. Bikson M, et al., Effects of uniform extracellular DC electric fields on excitability in rat hippocampal slices in vitro. J Physiol, 2004 557(Pt 1): p. 175–90. [PubMed: 14978199]
38. Radman T, et al., Role of cortical cell type and morphology in subthreshold and suprathreshold uniform electric field stimulation in vitro. Brain Stimul, 2009 2(4): p. 215–28, 228 e1–3. [PubMed: 20161507]

HIGHLIGHTS

- Electrokinetic transport may be directed along an electrical current path in tissue and hydrogels from distances of several hundred micrometers to millimeters.
- Amount of solute delivered depends on current.
- Technically similar to microiontophoresis, but the larger currents and longer times lead to greater solute penetration.

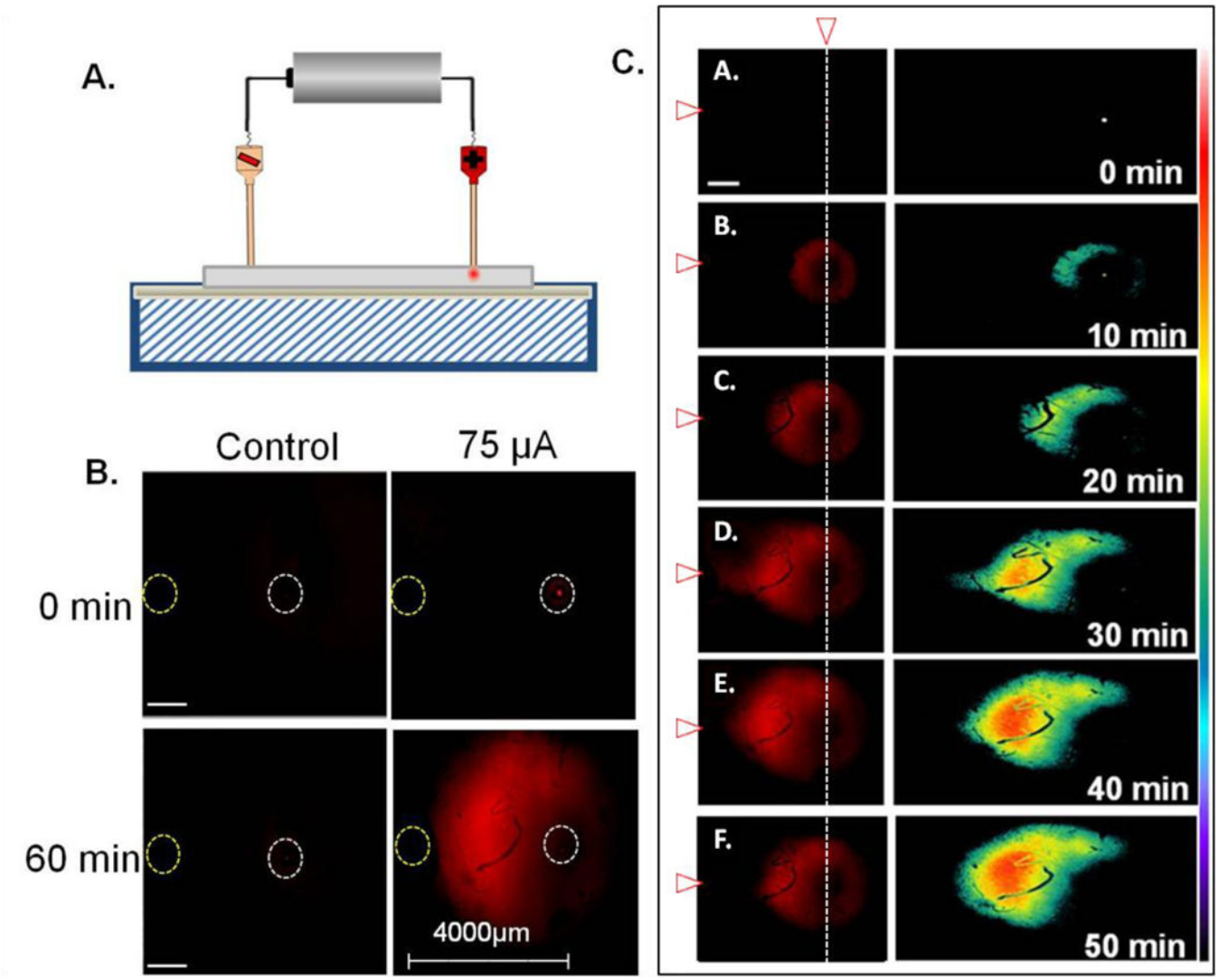

Figure 1.

Example of an electrokinetic infusion of $Ru(bpy)_3^{2+}$ in a hydrogel with a ζ-potential similar to rat OHSCs with 75 µA applied current for 60 minutes. (A) Experimental set-up. (B) Fluorescence in a hydrogel with an applied current of 75 µA. Left images are the control gel with no applied current and right images are after an applied current. (C) Infusion profiles were obtained at varying time points in a hydrogel, with an applied current of 75 µA. Top panel is at time 0 and bottom panel is at time 50 minutes. Scale bar in C is 100 µm. Corresponding surface intensity (right column) plots were also examined with fluorescence images as shown in C. The color bar to the right represents relative intensity with white (255) and black (0). White vertical dotted line shows the position of dye and infusion capillary and white/red arrow represents the position of the counter capillary/electrode (left). An Olympus objective lens of 1.25× with a numerical aperture of 0.04 was used for imaging.

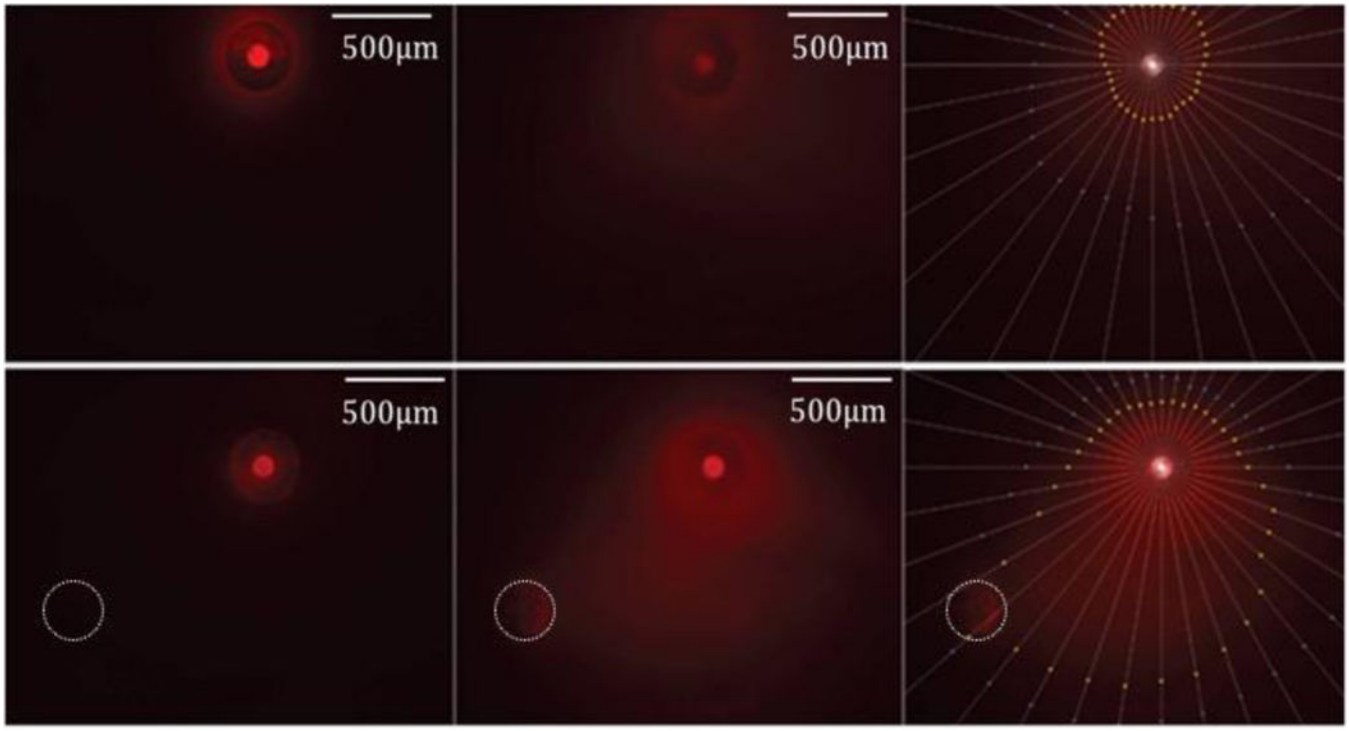

Figure 2.

Delivery of $Ru(bpy)_3^{2+}$ in OHSCs at 1.5μA current. Left column is at initial timepoint; Center column is after 25 minutes; Right column is after 25 minutes with points showing 25% (yellow) and 15% (blue) of the maximum intensity at the infusion capillary. Top row: counter electrode in the GF-HBSS bath below the tissue. Bottom row: counter electrode at lower left in tissue, denoted with white outline. The scale bar is 500 μm.

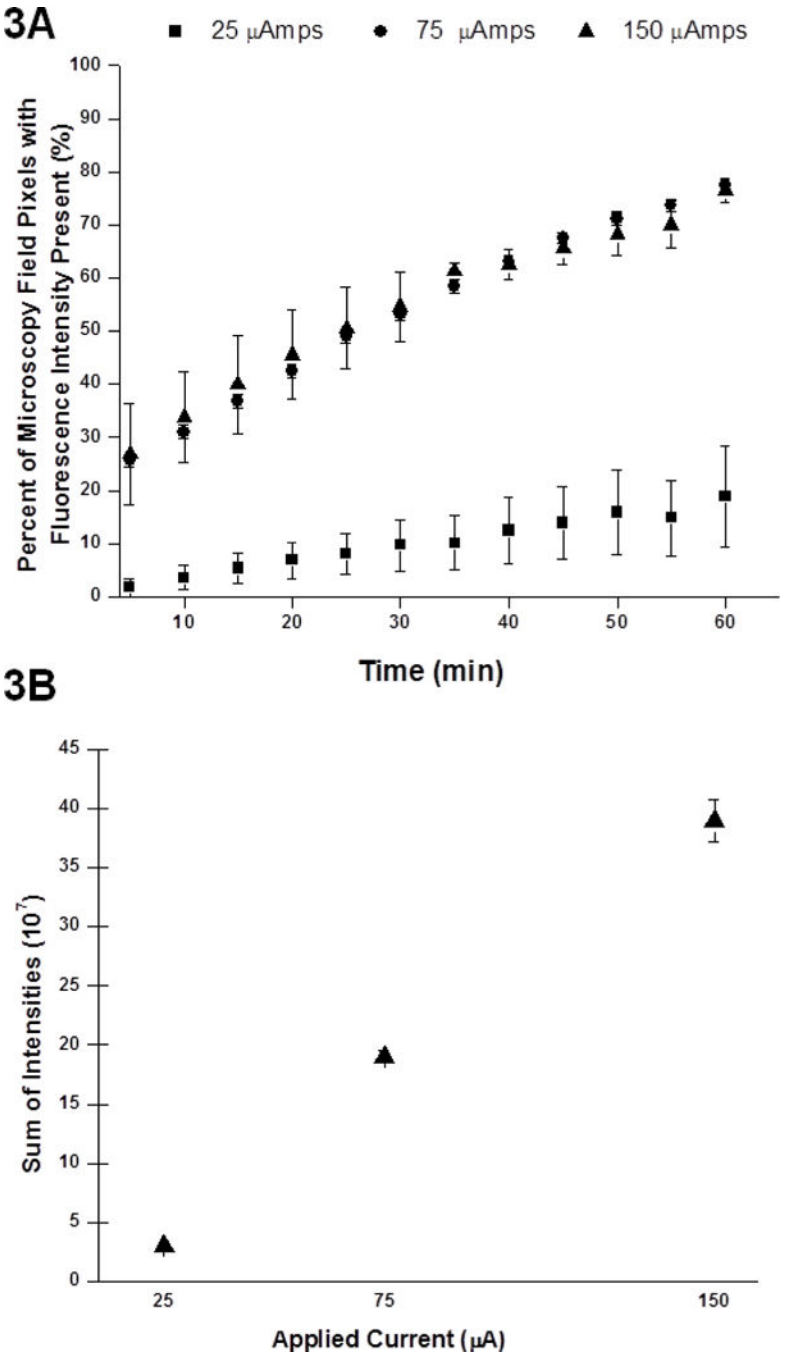

Figure 3.

Electrokinetic transport of $Ru(bpy)_3^{2+}$ in a hydrogel model of brain tissue using 3 different currents: 25 μA, 75 μA and 150 μA for 1 hour *(N* = 3 each). (A) Percentage of pixels in viewing area at a magnification of 1.25x demonstrating fluorescence intensity above background. Significant difference exists between 25 μA and 75 μA and between 25 μA and 150 μA. One-way ANOVA: F (2,33) = 41.36, $p = 0.000001$; and Tukey post-hoc test: $p<0.05$. (B) Aggregate sum of fluorescence intensity above background within viewing area

at a magnification of 1.25× with numerical aperture 0.04. Significant differences exist between the three currents with error bars representing standard error of the mean (SEM).